Organic & Biomolecular Chemistry

Cite this: *Org. Biomol. Chem.*, 2012, **10**, 7552

www.rsc.org/obc

PAPER

Modelling peptide–metal dication interactions: formamide–Ca^{2+} reactions in the gas phase

Ane Eizaguirre,[a] Otilia Mó,[a] Manuel Yáñez,*[a] Jean-Yves Salpin*[b,c] and Jeanine Tortajada[b,c]

Received 18th June 2012, Accepted 24th July 2012
DOI: 10.1039/c2ob26166a

The collision induced dissociation of formamide–Ca^{2+} complexes produced in the gas phase through nanoelectrospray ionization yields as main products ions $[CaOH]^+$, $[HCNH]^+$, $[Ca(NH_2)]^+$, HCO^+ and $[Ca(NH_3)]^{2+}$ and possibly $[Ca(H_2O)]^{2+}$ and $[C,O,Ca]^{2+}$, the latter being rather minor. The mechanisms behind these fragmentation processes have been established by analyzing the topology of the potential energy surface by means of B3LYP calculations carried out with a core-correlated cc-pWCVTZ basis set. The Ca^{2+} complexes formed by formamide itself and formimidic acid play a fundamental role. The former undergoes a charge separation reaction yielding $[Ca(NH_2)]^+ + HCO^+$, and the latter undergoes the most favorable Coulomb explosion yielding $[Ca–OH]^+ + [HCNH]^+$ and is the origin of a multistep mechanism which accounts for the observed loss of water and HCN. Conversely, the other isomer of formamide, amino(hydroxyl)carbene, does not play any significant role in the unimolecular reactivity of the doubly charged molecular cation.

Introduction

Formamide can be considered as the simplest prototype model of a peptide function. Hence, many studies on the gas-phase reactivity of this small compound with different reactants, in particular metal cations, have been reported in the literature.[1–13] However, most of these investigations were focused on singly charged species,[4,6–8,10] and the information on formamide reactivity with doubly or multiply charged species is scarce and fragmentary.[9,11–13] Indeed, although previous studies on the interactions between Ca^{2+} and base-pairs[14–19] and nucleic acid bases[20] have been reported in the literature, studies specifically dealing with formamide–Ca^{2+} interactions are very rare,[21] most of them related to the role of formamide as a detubulation agent.[22–24] On top of that formamide is also a molecule of astrobiological interest, which has been identified in cometary coma and interstellar ices and is considered a precursor in the abiotic synthesis of amino acids.[25] Consequently, many works focused their attention on the spectroscopic properties of this compound and its derivatives,[26–28] and on its formation or reactivity on ices and other materials.[29,30] Formamide also constitutes a good model to investigate proton exchange processes in peptides, proteins and base-pairs,[31,32] amide hydrolysis[33] or to mimic tautomerization processes[2,4,6,8] which may take place in more complex systems such as guanine, and which lead to what are usually known as the rare tautomers. In this respect, it should be mentioned that the two isomers of formamide which can be generated by the appropriate hydrogen shifts, namely formimidic acid and amino(hydroxy)carbene (see Scheme 1), have been actually generated and detected in the gas phase through the use of neutralization–reionization experiments.[34]

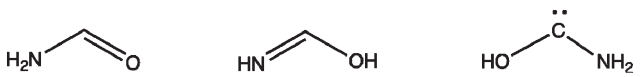

Scheme 1

The effect of different singly-charged metal ions, namely Li^+, Na^+, Mg^+, Al^+ or Cu^+, on the tautomerization processes connecting formamide with its aforementioned isomers was also reported in the literature.[4,6,8] Actually, the formimidic acid normally plays a significant role in gas-phase formamide reactivity with metal ions because the formation of the enol involves activation barriers typically below the energy of the entrance channel.[7,10] However, to the best of our knowledge, the effect of doubly-charged metal ions on the formamide → formimidic acid isomerization process has been only explored[13] for the particular case of Sr^{2+} whereas no information whatsoever is available regarding the possible catalytic effects of doubly-charged metal ions on the formamide → amino(hydroxy)carbene or on the formimidic → amino(hydroxy)carbene tautomerization processes. Hence, the aim of this paper is to explore both the intrinsic reactivity of formamide when the reference acid is Ca^{2+}, and

[a]*Departamento de Química, Módulo 13, Facultad de Ciencias, Universidad Autónoma de Madrid, Campus de Excelencia UAM-CSIC, Cantoblanco, 28049, Madrid, Spain. E-mail: manuel.yanez@uam.es*
[b]*Université d'Evry Val d'Essonne – Laboratoire Analyse et Modélisation pour la Biologie et l'Environnement (LAMBE) – Bâtiment Maupertuis, Boulevard François Mitterrand, 91025 Evry, France*
[c]*CNRS, UMR 8587, France. E-mail: jean-yves.salpin@univ-evry.fr*

the effect that this doubly-charged metal ion may have on the tautomerization processes connecting formamide, formimidic acid and amino(hydroxy)carbene among them. The investigation of the reactivity will be carried out by combining electrospray ionization/mass spectrometry techniques with high-level density functional theory (DFT) calculations. The survey of the possible catalytic effect of Ca^{2+} on the formamide tautomerization processes will be carried out exclusively on theoretical grounds.

Ca^{2+} is ubiquitous in the physiological media and is responsible for many phenomena in this medium. Just to mention some of them, Ca^{2+} contributes to increase the base-pair dissociation energy,[35] favors proton transfer between guanine and cytosine,[35] leads to an assisted intramolecular proton transfer in uracil dimers,[36] regulates muscle contraction,[37,38] increases the melting temperature of the DNA double helix or thermally stabilizes the proteins.[39]

Experimental and computational details

Experimental section

Electrospray MS/MS mass spectra were recorded on a QSTAR PULSAR i (Applied Biosystems/MDS Sciex) QqTOF instrument fitted with a nanoelectrospray source. 6 μL of a 1 : 1 aqueous mixture of calcium chloride and formamide (10^{-3} mol L^{-1}) were typically nanosprayed (20–50 nL min^{-1}) using borosilicate emitters (Proxeon). The sample was ionized using a 900 V nanospray needle voltage and the lowest possible nebulizing gas pressure (tens of millibars). The declustering potential DP (also referred to as "cone voltage" in other electrospray interfaces), defined as the difference in potentials between the orifice plate and the skimmer (grounded), ranged from 0 to 60 V. The pressure of the curtain gas (N_2), which prevents air or solvent from entering the analyzer region, was adjusted to 0.7 bar by means of pressure sensors, as a fraction of the N_2 inlet pressure. To improve ion transmission and subsequent sensitivity during the experiments, the collision gas (CAD, N_2) was present at all times for collisional focusing in both the Q0 (ion guide preceding the quadrupole Q1 and located just after the skimmer) and Q2 (collision cell) sectors.

For MS/MS spectra, complexes of interest were mass-selected using Q1, and allowed to collide with nitrogen (collision gas) in the second quadrupole (Q2), the resulting product ions being analyzed by the time-of-flight (TOF) after orthogonal injection. Furthermore, MS/MS spectra were systematically recorded at various collision energies ranging from 7 eV to 20 eV in the laboratory frame (the collision energy is given by the difference between the potentials of Q0 and Q2). The CAD parameter, which roughly controls the amount of N_2 introduced into Q2, was set to its minimum value in order to limit multiple ion–molecule collisions. Note that setting the CAD parameter to 1 during MS/MS experiments resulted in pressure values of 1–2 × 10^{-5} Torr as measured by the ion gauge located outside the collision cell. However, the pressure inside the collision cell is in fact of the order of 10 mTorr.[40] At this pressure and given the dimension of the LINAC collision cell (~22 cm long), the mean free path for a N_2 molecule is about 5 mm. So, not only the N_2 molecule but also complexes of interest (which have higher collision cross-sections) may undergo tens of collisions along their path through Q2. Consequently, we are certainly under a multiple collision regime even with the minimum amount of N_2 inside the collision cell (CAD = 1).

All experiments were performed in 100% water purified with a Milli-Q water purification system. Formaldehyde and calcium chloride were purchased from Aldrich (St Quentin-Fallavier, France) and were used without further purification.

Computational details

The theoretical model adopted for our survey of the formamide–Ca^{2+} potential energy surface (PES) was shown in the literature to provide results of similar accuracy as those obtained through the use of G3 and W1C and W2C high-level *ab initio* calculations.[41] This procedure is based on the use of geometries optimized using the hybrid functional B3LYP,[42,43] as implemented in the Gaussian 09 suite of programs,[44] in conjunction with the correlation-consistent polarized core-valence triple-zeta cc-pWCVTZ basis set.[45] It should be noted that the cc-pWCVTZ basis set includes core-correlation functions, since it has been shown that the inclusion of core-correlation effects is important for the accurate treatment of alkaline earth metal oxides and hydroxides.[46,47] The same level of theory was employed to calculate the final energies and the corresponding harmonic vibrational frequencies, which allowed us to classify the different stationary points on the PES either as local minima (no imaginary frequencies) or transition states (TS) when the structure presents one imaginary frequency. These harmonic frequencies were also used to estimate the zero point vibrational energy (ZPVE) corrections. The calculated interaction energies were not corrected however with the basis set superposition error (BSSE), which has been shown to be very small when the aforementioned level of theory is employed.[41] The connectivity between the different transition states and their adjacent minima was unambiguously established by using the intrinsic reaction coordinate (IRC) approach, as implemented in the Gaussian-09 series of programs.[44]

The bonding in the different structures involved in the formamide–Ca^{2+} PES was analyzed by means of the atoms-in-molecules (AIM) theory.[48] For this purpose, we have located the corresponding bond critical points (BCPs) and calculated the electron density values at the BCP position, since these values provide a quantitative measure of the bond strength, and together with other indexes, such as the energy density, also permit us to obtain useful information about the electrostatic or covalent character of the interactions. All these calculations have been carried out with the AIMPAC series of programs.[49]

A complementary view can be obtained by means of the electron localization function (ELF), initially proposed by Becke and Edgecombe.[50] This approach leads to the definition of basins, as regions of the space associated with electron pairs. Accordingly, these basins are usually classified as monosynaptic when they are associated to core-pairs or to lone-pairs of electrons, and disynaptic (or polysynaptic) when they have contributions from the valence shell of two (or more) atoms, and therefore are associated with bonding pairs of electrons. Indeed, ELF may provide useful information on bonding patterns in challenging cases in which other approaches fail to give an unambiguous bonding

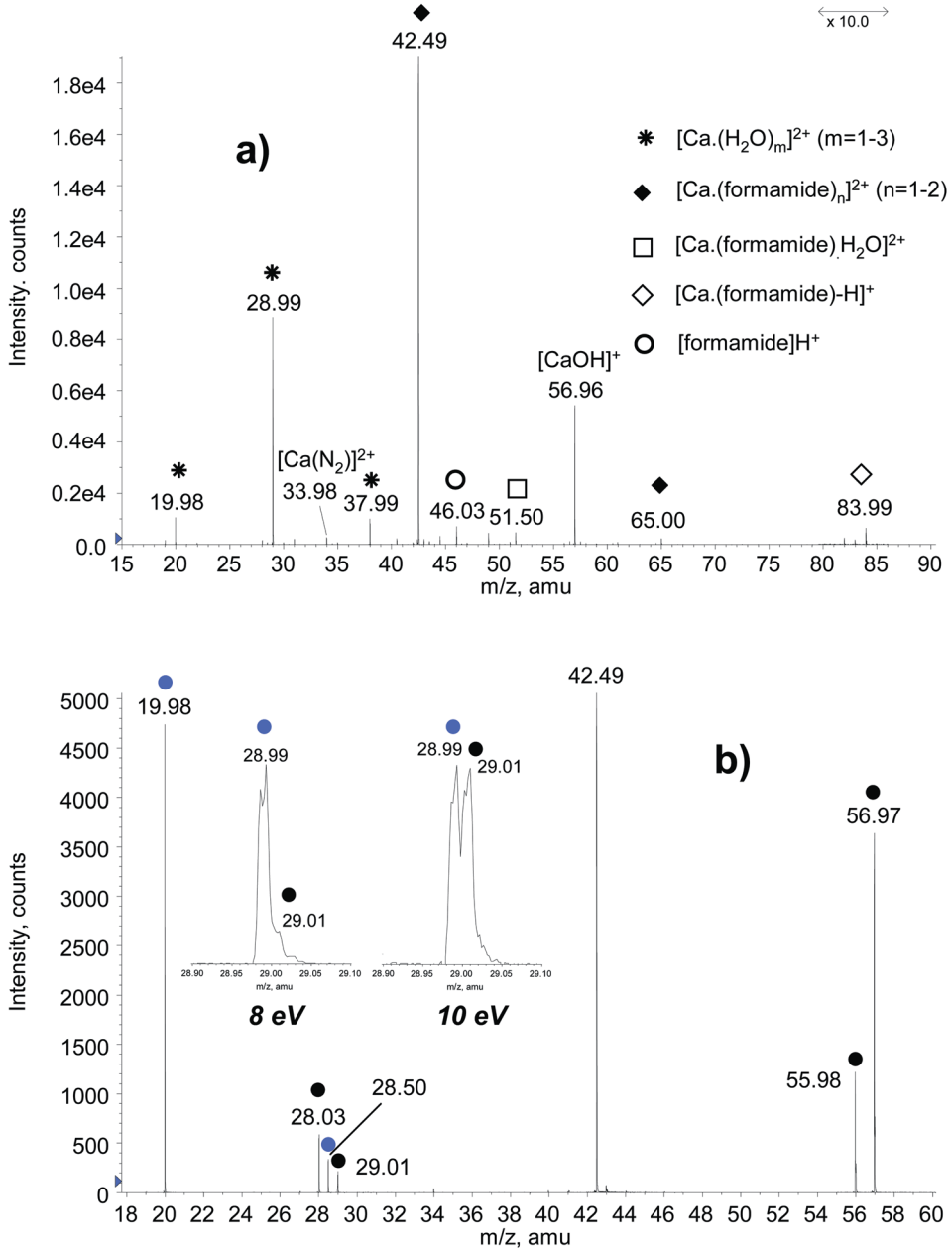

Fig. 1 (a) Positive nanoelectrospray spectrum of an aqueous $CaCl_2$/formamide (10^{-3} mol L^{-1}/10^{-3} mol L^{-1}) mixture, recorded with a declustering potential of 20 V. (b) Low-energy CID spectra of the [Ca(formamide)]$^{2+}$ complex recorded with a collision energy of 11 eV (laboratory frame), except the insert. See text for details.

picture, as it is for instance the case for iminoboranes[51] or selenocyanates.[52] ELF calculations were carried out with the TopMod suite of programs.[53]

Results and discussion

Experimental results

Fig. 1a shows the nanoelectrospray spectrum obtained with an equimolar aqueous mixture of calcium chloride and formamide (10^{-3} mol L^{-1}). First, no ions were detected above *m*/*z* 100. Chlorine-containing species were not detected, regardless of the interface conditions used.

Careful examination of this spectrum reveals the formation of both singly- and doubly-charged ions. As already observed for other ligands such as urea,[54] glycine[55] or uracil,[56] setting the DP parameter to a low voltage results in the abundant production of doubly-charged species. At DP = 0 V, the mass spectrum is characterized by prominent hydrated calcium ions ([Ca-$(H_2O)_m$]$^{2+}$; m = 1–3) detected at *m*/*z* 28.99, 37.99 (base peak) and 47.00. Calcium hydroxide $[CaOH]^+$ (*m*/*z* 56.96) is also highly abundant. Bare Ca^{2+} (*m*/*z* 19.98) and [Ca(formamide)]$^{2+}$ (*m*/*z* 42.49) are already observed at this DP value. The latter becomes the base peak at DP = 20 V (Fig. 1a) while the abundance of hydrated calcium ions quickly drops as DP increases. Two other dications, namely [Ca(formamide)·H_2O]$^{2+}$

(m/z 51.50) and $[Ca(formamide)_2]^{2+}$ (m/z 65.00), are detected, albeit in weak abundance. Finally, due to the presence of N_2 along the ion path for collisional focusing, $[Ca(N_2)]^{2+}$ ions (m/z 33.98) are also observed. Apart from calcium hydroxide, only two singly-charged ions are detected. Their intensity is particularly weak and is not improved when increasing the DP parameter. The first one is protonated formamide (m/z 46.03). The second one, observed at m/z 83.99, arises from the interaction between the metal and formamide and corresponds to the $[Ca(formamide)–H]^+$ complex. Its abundance is particularly small if one compares with the electrospray spectrum that we obtained with urea,[54] for which the $[Ca(urea)–H]^+$ ion was the most abundant species formed from Ca^{2+} and urea, regardless of the DP value used. This difference can be attributed to the formation for urea of abundant $[Ca(urea)_n]^{2+}$ ions ($n \geq 2$), which easily dissociate through dissociative proton transfer in the interface region to generate the $[Ca(urea)–H]^+$ ion.

We set the DP parameter at 35 V to record the MS/MS spectra of the $[Ca(formamide)]^{2+}$ complex, the CAD parameter being set to its minimum value (1). Opting for a higher value (2 and above) resulted in trace amounts of water within Q2 leading to the detection of the $[Ca(formamide)\cdot H_2O]^{2+}$ complex (m/z 51.50), which, upon collision, gives rise to protonated formamide (m/z 46.03). These two peaks disappear when CAD is set to 1.

On our instrument and for this particular system, the smallest collision energy in the laboratory frame (E_{lab}) for which sufficient amounts of fragment ions can reach the detector was 7 eV, and at this value dissociation of the precursor ions already occurs. E_{lab} was scanned from 7 to 20 eV, N_2 being used as a target gas. This corresponds, for the doubly-charged complex $[Ca(formamide)]^{2+}$, to center-of-mass collision energies (E_{CM}) ranging from 3.47 to 9.91 eV. The CID spectrum obtained at 11 eV (laboratory frame) is given in Fig. 1b. MS/MS spectra were recorded from m/z 15 up to m/z 120. However, no fragment ions were detected above m/z 60. Examination of this spectrum shows that the doubly-charged complex dissociates according to two types of processes, leading either to new dications by neutral losses, or to singly charged species, through charge separation processes (Scheme 2).

Three dications are indeed detected, namely $[Ca(NH_3)]^{2+}$ (m/z 28.50), $[Ca(H_2O)]^{2+}$ (m/z 28.99) and bare Ca^{2+} (m/z 19.96), which correspond to the elimination of carbon monoxide,

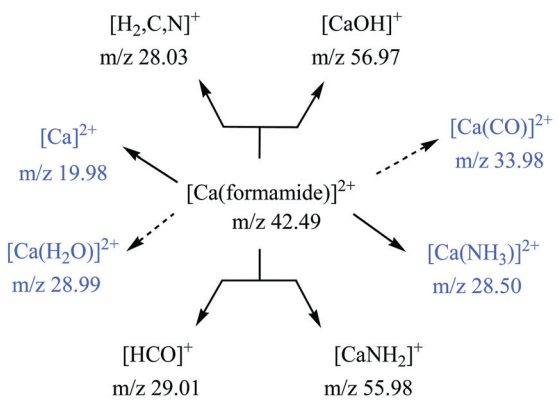

Scheme 2

[H,C,N] and intact formamide, respectively. Note that the presence of hydrated calcium on the MS/MS spectrum might also be imparted to interaction of Ca^{2+} with trace amounts of water present in the collision cell. A fourth doubly-charged ion is also detected at m/z 33.98 but in trace amounts. This latter species might correspond to the formation of the $[Ca(CO)]^{2+}$ (theoretical m/z of 33.979) ions through the elimination of NH_3. Consequently, the detection of both $[Ca(NH_3)]^{2+}$ and $[Ca(CO)]^{2+}$ would suggest the formation of an intermediate in which the metallic centre would interact with both ammonia and carbon monoxide. This assumption is supported by the presence of both $[Sr(NH_3)]^{2+}$ and $[Sr(CO)]^{2+}$ when studying the MS/MS spectrum of the $[Sr(formamide)]^{2+}$ complex.[13] However, the m/z 33.98 ion presently might also correspond to the $[Ca(N_2)]^{2+}$ complex (theoretical m/z of 33.984) which appears isobaric of $[Ca(CO)]^{2+}$ given the resolving power of the instrument. The $[Ca(N_2)]^{2+}$ complex has already been unambiguously observed during the study of $[Ca(H_2O)_n]^{2+}$ complexes.[57]

Two charge-separation processes are presently observed, leading to two pairs of singly-charged fragments, 28.03/56.97 and 29.01/55.98, that can be interpreted as $[H_2,C,N]^+/[CaOH]^+$ and $[HCO]^+/[Ca(NH_2)]^+$, respectively. The insert of Fig. 1b shows that two distinct ions are detected in the vicinity of m/z 29, and $[HCO]^+$ becomes dominant as the collision energy is increased.

While partner peaks arising from such processes should have in principle the same intensity, the lightest ions are systematically less intense than the heaviest ones, as already observed for other Ca^{2+}-containing[54–56,58] or Sr^{2+}-containing[13] systems. This was attributed to differences in radial ion energies, the lighter ions generated by the Coulomb explosion gaining most of the radial energy and therefore having a much higher velocity than the heaviest fragment. This can result in unstable ion trajectories, especially with a QqTOF instrument and its orthogonal geometry, and explains why lighter ions are more discriminated onto the MS/MS spectrum.

The most abundant fragment ions are Ca^{2+} and $[CaOH]^+$, regardless of the collision energy. At low collision energy (below 10 eV), calcium hydroxide $[CaOH]^+$ (m/z 56.97) is the most intense fragment ion, while Ca^{2+} ion is detected but to a lesser extent. However, the abundance ratio of these two ions quickly reverses, because of the sharp increase of the Ca^{2+} intensity with the collision energy. $[Ca(formamide)]^{2+}$ and $[Sr(formamide)]^{2+}$ complexes share several common fragmentations, such as the formation of M^{2+} and $[M(NH_3)]^{2+}$ ions or the charge-separation process leading to the metal hydroxide. On the other hand, detection of a hydrated dication is only observed for strontium,[13] while metal insertion into the prototype peptidic bond, leading to HCO^+ and $[M(NH_2)]^+$, is specific of the calcium unimolecular reactivity. Note that the $[Ca(NH_2)]^+$ species has also been observed for the $[Ca(urea)]^{2+}$ complex. On the other hand, elimination of [H,N,C,O] does not occur with formamide. The behavior upon collision of the $[Ca(formamide)]^{2+}$ ion can also be compared with that of singly-charged complexes. The dissociation of the $[Ni(formamide)]^+$ complex has been studied under metastable and low-energy CID conditions,[10] and loss of intact formamide has been observed under both conditions. This process is also encountered for the Cu^+/formamide system.[7] On the other hand, both dehydrogenation, loss of ammonia and dehydration are exclusively observed

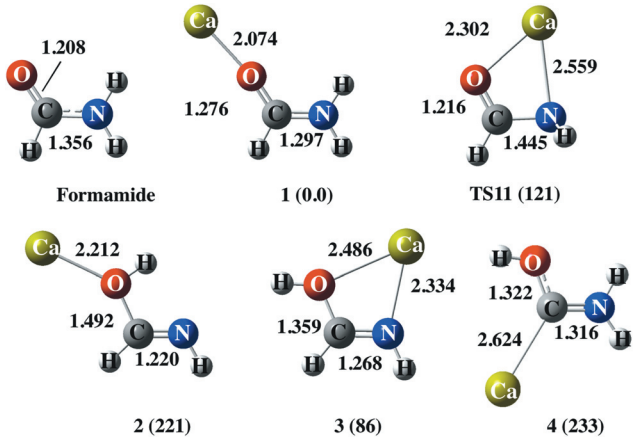

Fig. 2 Optimized geometries of the complexes formed by the association of Ca^{2+} to formamide, formimidic acid and amino(hydroxy)-carbene. Relative energies are in kJ mol^{-1}. The structure of formamide is also included for the sake of comparison.

with the transition metals. We also recorded the MS/MS spectrum of the singly-charged [Ca(formamide)–H]$^+$ ion (not shown). It turns out that the formal removal of one hydride from the doubly-charged complex results in a very different unimolecular reactivity, mostly characterized by dehydrogenation and elimination of [H,C,N], and therefore rather similar to the reactivity of the transition metal complexes. Finally, we can deduce from MS/MS experiments that the ion detected at *m/z* 65.00 is in fact a mixture of two species, namely $[Ca(H_2O)_5]^{2+}$ and $[Ca(formamide)_2]^{2+}$. The dissociation pattern of this latter bisligated doubly-charged complex is classical, with elimination of a neutral ligand (*m/z* 42.49) and charge reduction by interligand proton transfer giving rise to protonated formamide (*m/z* 46.03) and the [Ca(formamide)–H]$^+$ ion (*m/z* 83.99).

Structure and bonding of formamide–, formimidic acid– and amino(hydroxy)carbene–Ca^{2+} complexes. The B3LYP/cc-pWCVTZ optimized geometries and the relative energies of the complexes formed by attachment of Ca^{2+} to formamide, formimidic acid and amino(hydroxy)carbene are shown in Fig. 2. This figure includes also the optimized structure of the isolated neutral systems for the sake of comparison. As has been found before in the literature, formimidic acid and amino(hydroxy) carbene lie 46 and 153 kJ mol^{-1} higher in energy than formamide. All energies discussed hereafter include the ZPE correction.

The association of Ca^{2+} to formamide yields a complex, **1**, in which the doubly-charged metal ion attaches to the carbonyl oxygen. It is worth noting that although the interaction is essentially electrostatic, as reflected in the small values of the electron density at the BCP between the metal and the basic site and in the absence of a disynaptic basin involving the valence shell of the metal ion and that of the carbonyl oxygen (see Fig. 3), there is a sizably large polarization of the electron density of the base, which enhances the conjugation of the amino lone-pair with the C═O bond.

This is nicely reflected by the changes in the ELF, as well as in the increase of the electron density at the C–N BCP, which results in a significant shortening of the bond (see Fig. 2 and 3). However, in contrast with what has been found when the reference acid is Cu^+,[7] the association of Ca^{2+} to the amino group is not a local minimum of the PES, as it evolves to a structure in which Ca^{2+} bridges between the carbonyl and the amino groups, but which is a transition state (**TS11**), which connect the global minimum with itself, in a kind of circular orbiting of the metal cation, in agreement with what was found for Sr^{2+}.[59]

The association of Ca^{2+} to formimidic acid yields two different complexes, namely structures **2** and **3**, the most stable one being that in which the metal dication bridges between the two basic sites of the neutral, reflecting the low intrinsic basicity of the OH group. Importantly however, in both cases the energy gap with respect to formamide increases upon Ca^{2+} attachment. Similar findings were reported for some singly-charged metal ions, namely Li^+, Na^+, Mg^+, Al^+, even though in these cases the destabilization observed is smaller (67 kJ mol^{-1}, in average)[4] than that predicted for Ca^{2+} (86 kJ mol^{-1}). The smaller relative stability of structure **3** was actually explained as a direct consequence of the electrostatic nature of the interactions between the base and the metal ion.[4] On going from formamide to formimidic acid and to amino(hydroxy)carbene there is a significant decrease of the dipole moment of the system, which also changes its direction, leading necessarily to smaller ion–dipole interactions. Not surprisingly then, the relative destabilization of structure **3** should be larger for Ca^{2+} than for the singly-charged metals, since the electrostatic effects are the larger the greater the charge of the cation. Conversely, the equivalent to structure **3** was found to be significantly stabilized with respect to structure **1** when the reference acid was Cu^+.[8] Actually, in this latter case Cu^+ does not bridge between the two basic centers and appears only attached to the imino nitrogen which is very basic. This preference reflects the non-negligible covalent character of the interactions with Cu^+ through a significant charge donation from the lone-pairs of the basic site towards the low-lying 4s empty orbital of the metal ion,[8] which does not occur when the reference acid is Ca^{2+}.

The same applies when dealing with amino(hydroxy)carbene. Its association to Cu^+ leads to significant stabilization of the system through the formation of a strong dative bond from the carbene lone-pair towards Cu^+. Consequently, the energetic gap with respect to formimidic acid decreases by 66 kJ mol^{-1},[8] whereas this gap increases by 40 kJ mol^{-1} when the reference acid is Ca^{2+}. Again this reflects the much lower polarity of the carbene, which leads to a rather low electron density at the Ca–C BCP (see Fig. 3) and to a rather large C–Ca bond distance.

Isomerization barriers. As far as the isomerization processes are concerned, and similarly to what has been found for Cu^+,[8] our calculations indicate that Ca^{2+} triggers an anticatalytic effect, since as shown in Table 1, all barriers increase upon Ca^{2+} attachment, this increase being larger than the one calculated when the metal cation is Cu^+. Although the values for Cu^+ and Ca^{2+} were not obtained at the same level of theory, it should be mentioned that in the assessment of the method used herein for Ca^{2+}, the energy differences with respect to G2 values were always smaller than 4 kJ mol^{-1}, so this comparison is still meaningful.

This is however in clear contrast with the catalytic effect exhibited by Ca^{2+} on the tautomerization processes of uracil and its thio- and seleno-derivatives.[60–62] Whereas in formamide the

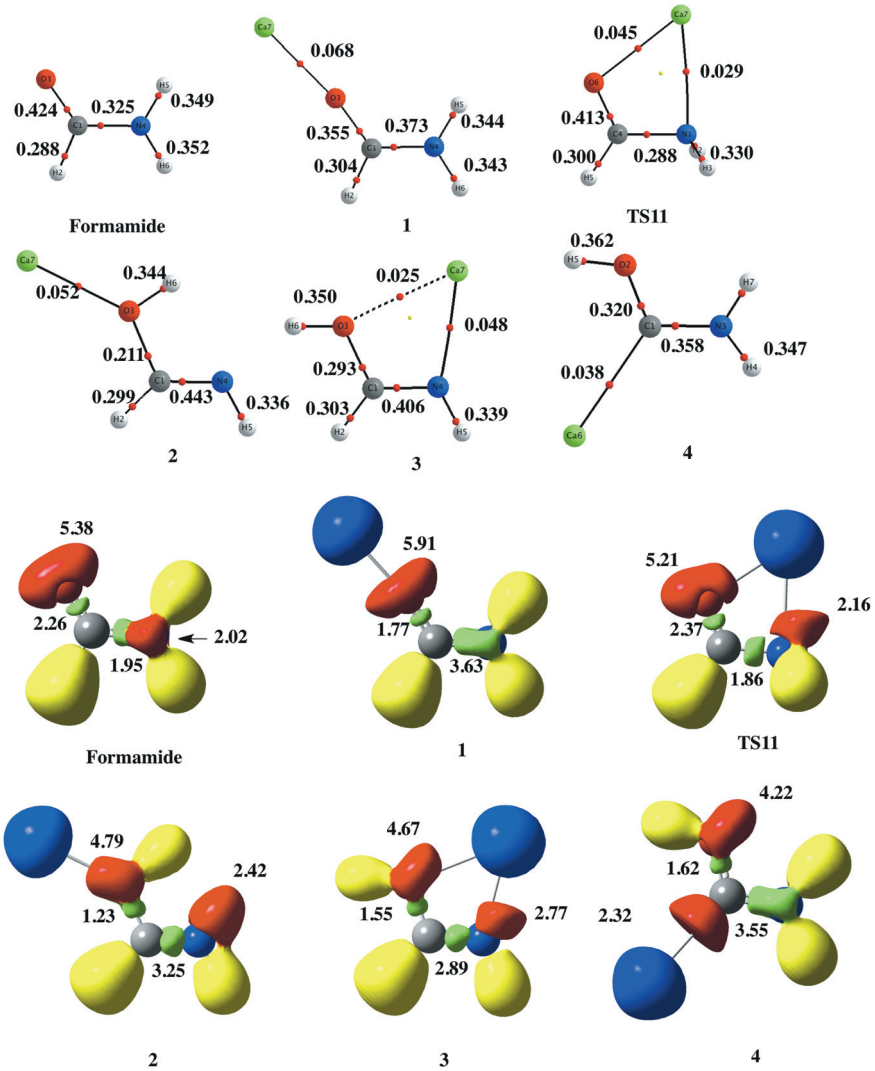

Fig. 3 Molecular graphs and ELF plots for the complexes formed by the association of Ca^{2+} to formamide, formimidic acid and amino(hydroxy)-carbene. The structure of formamide is also included for the sake of comparison. In the molecular graphs the red and yellow dots indicate the position of the BCPs and ring critical points, respectively. Electron densities are in a.u. In the ELF plots the blue, red, and green basins correspond to core-pairs, lone-pairs and bonding-pairs of electrons, respectively. The yellow basins are associated with chemical bonds involving H atoms. The populations of the basins are in e^-.

Table 1 Calculated activation barriers for the isomerizations between formamide and its isomers formimidic acid and amino(hydroxy)carbene and the effect produced by Cu^+ and Ca^{2+} association. All values in kJ mol^{-1}

Formamide → formimidic acid isomerization	Activation barriers
Neutral systems	172[a]
Cu^+ complexes	222[a]
Ca^{2+} complexes	264
Formamide → amino(hydroxy)carbene isomerization	
Neutral systems	303[a]
Cu^+ complexes	336[b]
Ca^{2+} complexes	388
Formimidic acid → amino(hydroxy)carbene isomerization	
Neutral systems	301[a]
Cu^+ complexes	348[b]
Ca^{2+} complexes	371

[a] Values calculated at the G2 level taken from ref. 4. [b] Values calculated at the B3LYP/6-311+G(2df,2p) taken from ref. 8.

enhanced acidity of the amino group in complex **1** is counterbalanced by the significant reduction of the basicity of the carbonyl group, whose electron density is strongly polarized towards the doubly-charged metal ion, disfavoring the proton transfer process, the existence of two carbonyl groups susceptible to enolization in the case of uracil changes completely the scenario, because the process which is actually catalyzed corresponds to the proton transfer towards the carbonyl group which is not interacting with the metal dication,[60–62] and whose intrinsic basicity is enhanced rather than reduced.

Collision induced dissociation mechanisms for formamide–Ca^{2+} complexes. As indicated in previous sections the direct attachment of Ca^{2+} to formamide yields exclusively adduct **1**, which will be necessarily the starting point of all possible fragmentation mechanisms. The mechanisms with origin in structure **1** are of two types, isomerization processes through the

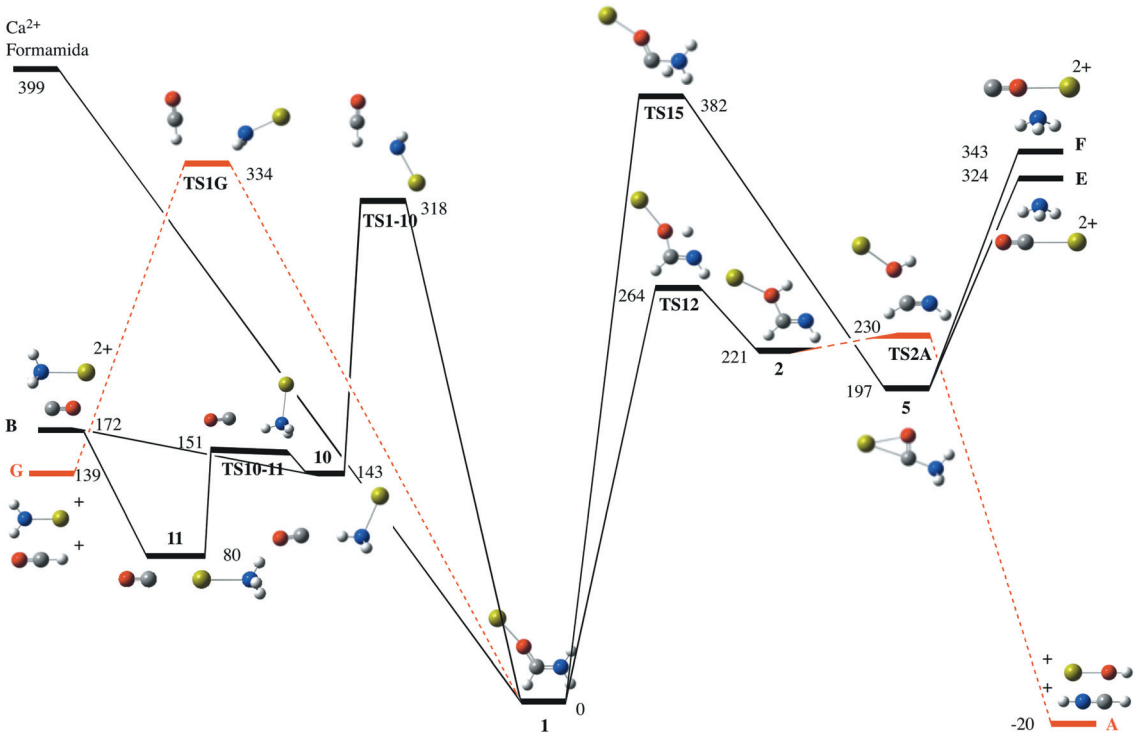

Fig. 4 Energy profile of the different reaction mechanisms with origin in the global minimum **1** of the formamide–Ca^{2+} PES. All values in kJ mol^{-1}.

appropriate hydrogen shifts and coulomb explosions in which the molecular dication splits into two lighter monocations. Among the latter the only possible mechanism is the one leading to $[Ca(NH_2)]^+ + HCO^+$ through the transition state **TS1G** (see Fig. 4).

It is worth noting that complex **1** is thermodynamically stable with respect to this coulomb explosion since the $[Ca(NH_2)]^+ + HCO^+$ exit channel lies 139 kJ mol^{-1} higher in energy. However, these two ions are actually observed in the MS/MS spectra corresponding to *m/z* values of 29.01 and 55.98, respectively (Fig. 1b). This is in agreement with the fact that the transition state involved in this process is 65 kJ mol^{-1} lower than the entrance channel. Interestingly, the same process is not observed in similar reactions between formamide and Sr^{2+}, even if the topology of the formamide–Sr^{2+} PES is rather similar to that of formamide–Ca^{2+}. The difference here is only quantitative, since Sr^{2+} is a much larger ion than Ca^{2+} the corresponding binding energy is lower, the global minimum **1** being only 332 kJ mol^{-1} below the entrance channel. Accordingly, while in formamide–Ca^{2+} the **TS1G** is significantly lower in energy than the entrance channel in formamide–Sr^{2+} this is no longer true and this transition state is almost isoenergetic with the entrance channel.

The global minimum can undergo one 1,3-H shift in which one of the amino hydrogens moves towards the carbonyl oxygen through the **TS12** transition state to yield the local minimum **2**, and one 1,2-H shift in which the amino hydrogen is transferred to the neighbor carbon atom through the **TS15** transition state to yield complex **5** (see Fig. 4). As is usually the case, this 1,2-H transfer involves a much higher barrier than the 1,3-H shift and therefore the formation of **2** should dominate over the formation of **5**. The formation of minimum **2** should be very easily followed by a coulomb explosion into $[CaOH]^+ + [HNCH]^+$, which besides being a rather exothermic process involves a very low energy barrier only 9 kJ mol^{-1} above structure **2** (see Fig. 4). This is in agreement with the high amounts of calcium hydroxide detected under MS/MS conditions, while the $[Ca(CO)]^{2+}$ ion, if actually generated (*vide supra*), is detected in very weak abundance.

Although the formation of structure **5** should be minority due to the high isomerization barrier needed to reach this local minimum (see Fig. 4), its fragmentation would produce a new doubly-charged species, namely $[Ca(CO)]^{2+}$ by the loss of a molecule of ammonia. The lower exit channel would correspond to the one in which Ca^{2+} is attached to the carbon atom of carbon monoxide. However, a more favorable process would be the one in which the doubly charged species formed is $[Ca(NH_3)]^{2+}$. The mechanism starts with the bond cleavage of the C–N bond of the global minimum with simultaneous displacement of the metal towards the N atom. The corresponding transition state, **TS1–10**, could apparently lead to a fragmentation into $[Ca(NH_2)]^+$ and HCO^+, but the corresponding IRC calculation shows that, instead, the proton attached to the HCO fragment is transferred to the N atom of the other fragment to finally yield complex **10**. Once the local minimum **10** is formed, its evolution towards a rather stable complex **11** is almost barrierless. Minimum **11** in which Ca^{2+} is bridging between NH_3 and CO leads to the loss of the latter, since the Ca–C linkage (bond length 2.722 Å) is significantly weaker than the Ca–N bond (bond length 2.491 Å). Hence the observed loss of NH_3 can only come from the fragmentation of minimum **5** discussed above.

We indicated above that minimum **2** may undergo a Coulomb explosion yielding $[CaOH]^+ + [HNCH]^+$. However, as illustrated in Fig. 5, competing with this coulomb explosion there is an

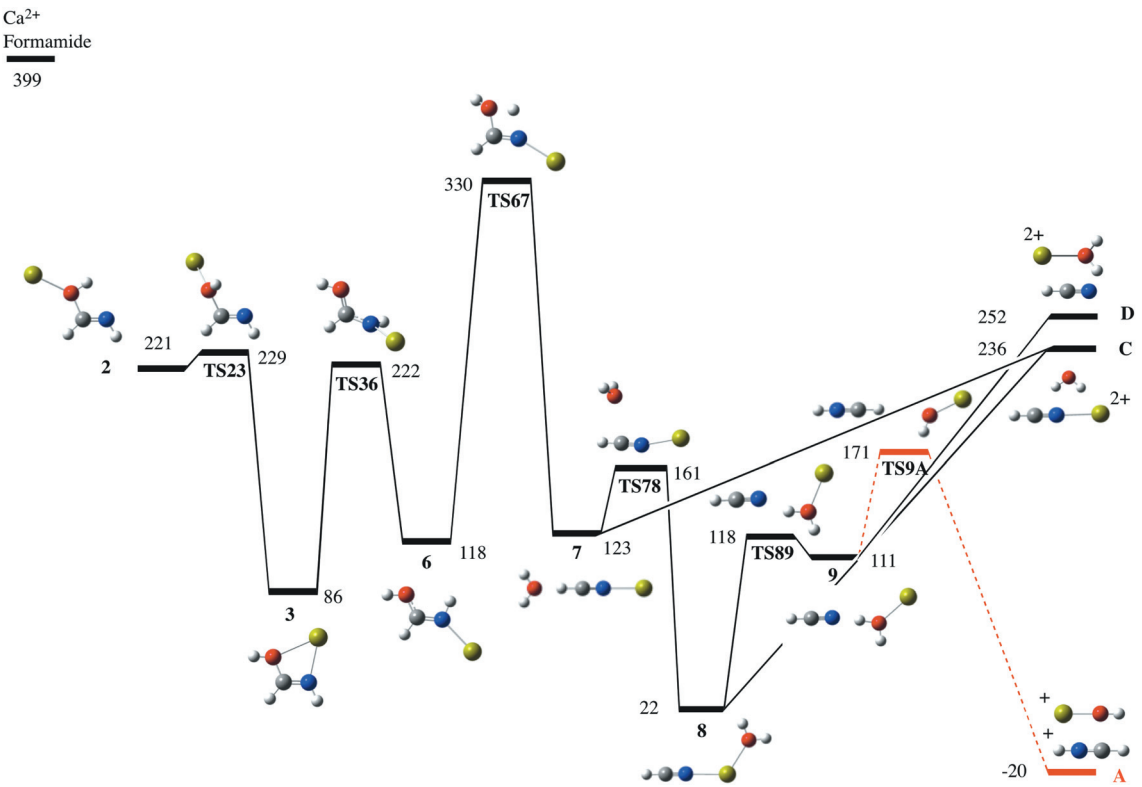

Fig. 5 Energy profile of the different reaction mechanisms with origin in the local minimum **2** of the formamide–Ca^{2+} PES. All values in kJ mol^{-1}.

internal rotation of the HOCa group around the C–O bond which leads to a much more stable isomer **3**, in which the Ca bridges between the carbonyl oxygen and the imino group and whose characteristics have been discussed above.

This new local minimum is the origin of a multistep mechanism which ends in the formation of another very stable local minimum **8**, in which the metal is simultaneously bound to HCN and to water. The cleavage of the Ca–water bond is more favorable by 16 kJ mol^{-1} than the cleavage of the bond between Ca and HCN, but since both exit channels are well below the entrance channel, two doubly-charged species $[Ca(HCN)]^{2+}$ and $[Ca(H_2O)]^{2+}$ should be formed in coincidence with the MS/MS experiments that present two peaks at *m/z* 33.49 and 28.99, respectively. Note that the loss of water and the subsequent formation of $[Ca(HCN)]^{2+}$ can also occur through the direct dissociation of local minimum **7** prior to its isomerization to yield **8**. In fact, it is worth mentioning that the $[Ca(H_2O)]^{2+}$ ion, although experimentally observed at low collision energy (Fig. 1b), might also originate from the interaction of abundant Ca^{2+} ions produced by CID with water present in trace amounts within the collision chamber. In addition, no $[Ca(HCN)]^{2+}$ ions were detected during the MS/MS experiments. Consequently, it seems reasonable to suggest that these dissociation processes, although globally exothermic, might not occur. This is consistent with the fact that they appear both kinetically and thermodynamically disfavored with respect to the formation of calcium hydroxide and protonated acetonitrile through **TS2A** (Fig. 4).

In the process of losing HCN from **8**, the intermediate complex **9**, in which the HCN moiety is hydrogen bonded to the H_2OCa fragment, can be formed. This opens the possibility of having a proton transfer from the latter to the former, through the **TS9A** transition state, in a charge separation process yielding $HCNH^+ + CaOH^+$, which are the same products found in the coulomb explosion of structure **2**.

Concluding remarks

Nanoelectrospray ionization/mass spectrometry experimental techniques show that the main products observed during collision induced dissociation of the formamide–Ca^{2+} complex are $[CaOH]^+$, $[HCNH]^+$, $[Ca(NH_2)]^+$, HCO^+ and $[Ca(NH_3)]^{2+}$ and possibly $[Ca(H_2O)]^{2+}$ and $[C,O,Ca]^{2+}$, the latter being rather minor. The formation of these products can be rationalized by analyzing the topology of the PES, in which formamide itself and formimidic acid play a fundamental role. The former yields upon Ca^{2+} attachment the global minimum **1** of the PES, which is responsible for one of the observed coulomb explosions yielding $[Ca(NH_2)]^+$ and HCO^+. Formimidic acid yields the local minimum **2** in which the metal cation is attached to its OH group and is produced through a 1,3-H shift from the global minimum. This structure plays a fundamental role, because it undergoes the most favorable coulomb explosion yielding $[CaOH]^+ + [HCNH]^+$.

The other isomer of formamide, amino(hydroxyl)carbene, does not play any significant role in the unimolecular reactivity of the doubly-charged molecular cation because its Ca^{2+} complexes lie very high in energy and the barriers involved in its formation are also very high.

We have also found that in contrast with the behavior of Cu^+ cations, but in coincidence with Li^+, Na^+, Mg^+ and Al^+ the association of Ca^{2+} to the two isomers of formamide, namely formimidic acid and amino(hydroxyl)carbene, increases the gaps between both of them and formamide, this effect being larger than the same effect observed for Li^+, Na^+, Mg^+ and Al^+, as would be expected from a typical electrostatic interaction. Also, Ca^{2+} attachment has an anticatalytic effect in the isomerization processes connecting the three aforementioned isomers.

Acknowledgements

This work has been partially supported by the DGI Project No. CTQ2009-13129-C01, by the Project MADRISOLAR2, Ref.: S2009PPQ/1533 of the Comunidad Autónoma de Madrid, by Consolider on Molecular Nanoscience CSC2007-00010, and by the COST Action CM0702. AE gratefully acknowledges a Ph.D. grant from the Ministerio de Ciencia e Innovación of Spain. A generous allocation of computing time at the CCC of the UAM is also acknowledged.

References

1 P. G. Jasien and W. J. Stevens, *J. Chem. Phys.*, 1986, **84**, 3271–3277.
2 X. C. Wang, J. Nichols, M. Feyereisen, M. Gutowski, J. Boatz, A. D. J. Haymet and J. Simons, *J. Phys. Chem.*, 1991, **95**, 10419–10424.
3 J. S. Kwiatkowski and J. Leszczynski, *J. Mol. Struct.*, 1992, **270**, 67–86.
4 J. Tortajada, E. Leon, J. P. Morizur, A. Luna, O. Mó and M. Yáñez, *J. Phys. Chem.*, 1995, **99**, 13890–13898.
5 O. N. Ventura, J. B. Rama, L. Turi and J. J. Dannenberg, *J. Phys. Chem.*, 1995, **99**, 131–136.
6 M. Alcamí, O. Mó, M. Yáñez, A. Luna, J. P. Morizur and J. Tortajada, *J. Phys. Chem. A*, 1998, **102**, 10120–10127.
7 A. Luna, B. Amekraz, J. Tortajada, J. P. Morizur, M. Alcamí, O. Mó and M. Yáñez, *J. Am. Chem. Soc.*, 1998, **120**, 5411–5426.
8 A. Luna, J. P. Morizur, J. Tortajada, M. Alcamí, O. Mó and M. Yáñez, *J. Phys. Chem. A*, 1998, **102**, 4652–4659.
9 M. Remko and B. M. Rode, *Chem. Phys. Lett.*, 2000, **316**, 489–494.
10 L. Rodriguez-Santiago and J. Tortajada, *Int. J. Mass Spectrom.*, 2002, **219**, 429–443.
11 J. M. Mercero, J. I. Mujika, J. M. Matxain, X. Lopez and J. M. Ugalde, *Chem. Phys.*, 2003, **295**, 175–184.
12 M. Remko and B. M. Rode, *Struct. Chem.*, 2004, **15**, 223–232.
13 A. Eizaguirre, O. Mó, M. Yáñez and J. Y. Salpin, *Phys. Chem. Chem. Phys.*, 2011, **13**, 18409–18417.
14 J. V. Burda, J. Sponer, J. Leszczynski and P. Hobza, *J. Phys. Chem. B*, 1997, **101**, 9670–9677.
15 J. Sponer, M. Sabat, J. V. Burda, J. Leszczynski and P. Hobza, *J. Phys. Chem. B*, 1999, **103**, 2528–2534.
16 M. Noguera, J. Bertran and M. Sodupe, *J. Phys. Chem. A*, 2004, **108**, 333–341.
17 W. L. Zhu, X. M. Luo, C. M. Puah, X. J. Tan, J. H. Shen, J. D. Gu, K. X. Chen and H. L. Jiang, *J. Phys. Chem. A*, 2004, **108**, 4008–4018.
18 J. Poater, M. Sodupe, J. Bertran and M. Sola, *Mol. Phys.*, 2005, **103**, 163–173.
19 M. Franska, *Eur. J. Mass Spectrom.*, 2007, **13**, 339–346.
20 N. Russo, M. Toscano and A. Grand, *J. Phys. Chem. A*, 2003, **107**, 11533–11538.
21 C. F. Chapman and M. Maroncelli, *J. Phys. Chem.*, 1991, **95**, 9095–9114.
22 F. Brette, K. Komukai and C. H. Orchard, *Am. J. Physiol. Heart Circ. Physiol.*, 2002, **283**, H1720–H1728.
23 J. Monterrubio, G. Ortiz, P. M. Orkand and C. Zuazaga, *J. Muscle Res. Cell Motil.*, 2002, **23**, 167–174.
24 S. Despa, F. Brette, C. H. Orchard and D. M. Bers, *Biophys. J.*, 2003, **85**, 3388–3396.
25 J. R. Brucato, G. Strazzulla, G. A. Baratta, A. Rotundi and L. Colangeli, *Origins Life Evol. Biosphere*, 2006, **36**, 451–457.
26 R. K. Khanna, M. S. Lowenthal, H. L. Ammon and M. H. Moore, *Astrophys. J. Suppl.*, 2002, **140**, 457–464.
27 M. Winnewisser, I. R. Medvedev, F. C. De Lucia, E. Herbst, J. Koput, K. Sastry and R. A. H. Butler, *Astrophys. J. Suppl.*, 2005, **159**, 189–195.
28 J. R. Brucato, G. A. Baratta and G. Strazzulla, *Astron. Astrophys.*, 2006, **455**, 395–399.
29 B. M. Jones, C. J. Bennett and R. I. Kaiser, *Astrophys. J.*, 2011, **734**, 78.
30 D. T. Halfen, V. Ilyushin and L. M. Ziurys, *Astrophys. J.*, 2011, **743**, 60.
31 C. L. Perrin, *Acc. Chem. Res.*, 1989, **22**, 268–275.
32 J. Bertran, A. Oliva, L. Rodriguez-Santiago and M. Sodupe, *J. Am. Chem. Soc.*, 1998, **120**, 8159–8167.
33 S. Antonczak, M. F. Ruiz-Lopez and J. L. Rivail, *J. Am. Chem. Soc.*, 1994, **116**, 3912–3921.
34 G. A. McGibbon, P. C. Burgers and J. K. Terlouw, *Int. J. Mass Spectrom. Ion Processes*, 1994, **136**, 191–208.
35 H. Sigel, *Chem. Soc. Rev.*, 1993, **22**, 255–267.
36 A. Eizaguirre, A. M. Lamsabhi, O. Mó and M. Yáñez, *Theor. Chem. Acc.*, 2011, **128**, 457–464.
37 P. J. Silver, J. Dachiw, J. M. Ambrose and P. B. Pinto, *J. Pharmacol. Exp. Ther.*, 1985, **234**, 629–635.
38 C. C. Ashley, T. J. Lea, I. P. Mullingan, R. E. Palmer and S. J. Simnett, *Adv. Exp. Med. Biol.*, 1993, **332**, 97–115.
39 A. A. Saboury, M. S. Atri, M. H. Sanati, A. A. Moosavi-Movahedi and K. Haghbeen, *Int. J. Biol. Macromol.*, 2005, **36**, 305–309.
40 I. V. Chernushevich, A. V. Loboda and B. A. Thomson, *J. Mass Spectrom.*, 2001, **36**, 849–865.
41 I. Corral, O. Mó, M. Yáñez, A. Scott and L. Radom, *J. Phys. Chem. A*, 2003, **107**, 10456–10461.
42 A. D. Becke, *J. Chem. Phys.*, 1993, **98**, 1372–1377.
43 C. Lee and R. G. Parr, *Phys. Rev. A: At., Mol., Opt. Phys.*, 1990, **42**, 193–200.
44 M. J. Frisch, G. W. Trucks, H. B. Schlegel, G. E. Scuseria, M. A. Robb, J. R. Cheeseman, G. Scalmani, V. Barone, B. Mennucci, G. A. Petersson, H. Nakatsuji, M. Caricato, X. Li, H. P. Hratchian, A. F. Izmaylov, J. Bloino, G. Zheng, J. L. Sonnenberg, M. Hada, M. Ehara, K. Toyota, R. Fukuda, J. Hasegawa, M. Ishida, T. Nakajima, Y. Honda, O. Kitao, H. Nakai, T. Vreven, J. A. Montgomery, Jr., J. E. Peralta, F. Ogliaro, M. Bearpark, J. J. Heyd, E. Brothers, K. N. Kudin, V. N. Staroverov, R. Kobayashi, J. Normand, K. Raghavachari, A. Rendell, J. C. Burant, S. S. Iyengar, J. Tomasi, M. Cossi, N. Rega, J. M. Millam, M. Klene, J. E. Knox, J. B. Cross, V. Bakken, C. Adamo, J. Jaramillo, R. Gomperts, R. E. Stratmann, O. Yazyev, A. J. Austin, R. Cammi, C. Pomelli, J. W. Ochterski, R. L. Martin, K. Morokuma, V. G. Zakrzewski, G. A. Voth, P. Salvador, J. J. Dannenberg, S. Dapprich, A. D. Daniels, O. Farkas, J. B. Foresman, J. V. Ortiz, J. Cioslowski and D. J. Fox, *GAUSSIAN09 (Revision A.02)*, Gaussian, Inc., Wallingford CT, 2009.
45 M. A. Iron, M. Oren and J. M. L. Martin, *Mol. Phys.*, 2003, **101**, 1345–1361.
46 A. Schulz, B. J. Smith and L. Radom, *J. Phys. Chem. A*, 1999, **103**, 7522–7527.
47 M. B. Sullivan, M. A. Iron, P. C. Redfern, J. M. L. Martin, L. A. Curtiss and L. Radom, *J. Phys. Chem. A*, 2003, **107**, 5617–5630.
48 R. F. W. Bader, *Atoms in Molecules. A Quantum Theory*, Clarendon Press, Oxford, 1990.
49 R. F. W. Bader and J. R. Cheeseman, *AIMPAC Programs*, 2000.
50 A. D. Becke and K. E. Edgecombe, *J. Chem. Phys.*, 1990, **92**, 5397–5403.
51 O. Mó, M. Yáñez, A. M. Pendas, J. E. Del Bene, I. Alkorta and J. Elguero, *Phys. Chem. Chem. Phys.*, 2007, **9**, 3970–3977.
52 C. Trujillo, O. Mó, M. Yáñez and B. Silvi, *J. Chem. Theory Comput.*, 2008, **4**, 1593.
53 S. Noury, X. Krokidis, F. Fuster and B. Silvi, *Comput. Chem.*, 1999, **23**, 597–604.
54 I. Corral, O. Mó, M. Yáñez, J. Y. Salpin, J. Tortajada and L. Radom, *J. Phys. Chem. A*, 2004, **108**, 10080–10088.
55 I. Corral, O. Mó, M. Yáñez, J. Y. Salpin, J. Tortajada, D. Moran and L. Radom, *Chem.–Eur. J.*, 2006, **12**, 6787–6796.
56 C. Trujillo, A. Lamsabhi, O. Mó, M. Yáñez and J. Y. Salpin, *Int. J. Mass Spectrom.*, 2011, **306**, 27–36.
57 I. Corral, C. Trujillo, J. Y. Salpin and M. Yáñez, in *Challenges and Advances in Computational Chemistry and Physics. Vol. 12 Kinetics and Dynamics: From Nano- to Bio-Scale*, ed. P. Paneth and A. Dybala-Defratyka, Springer, London, 2010, vol. 12.
58 C. Trujillo, O. Mó, M. Yáñez, J.-Y. Salpin and J. Tortajada, *ChemPhysChem*, 2007, **8**, 1330–1337.

59 A. Eizaguirre, O. Mó, M. Yáñez and J. Y. Salpin, *Phys. Chem. Chem. Phys.*, 2011, **13**, 18409–18417.
60 C. Trujillo, A. M. Lamsabhi, O. Mó, M. Yáñez and J. Y. Salpin, *Org. Biomol. Chem.*, 2008, **6**, 3695–3702.
61 A. M. Lamsabhi, O. Mó, M. Yáñez and R. J. Boyd, *J. Chem. Theory Comput.*, 2008, **4**, 1002–1011.
62 A. Eizaguirre, O. Mó, M. Yáñez and R. J. Boyd, *Org. Biomol. Chem.*, 2011, **9**, 423–431.